Int. J. Multiphase Flow Vol. 14, No. 2, pp. 141–154, 1988
Printed in Great Britain.

0301-9322/88 $3.00 + 0.00

PREDICTION OF TURBULENT, STRATIFIED, TWO-PHASE FLOW IN INCLINED PIPES AND CHANNELS

R. I. ISSA

Petroleum Engineering, Department of Mineral Resources Engineering, Imperial College of Science and Technology, London, England

(*Received* 28 *April* 1987; *in revised form* 28 *October* 1987)

Abstract—A method for the prediction of fully-developed, turbulent, stratified, two-phase flow in horizontal and inclined pipes and channels is presented. The method solves the two-dimensional momentum equations for both phases and accounts for the effects of turbulence through the use of the k–ϵ two-equation model of turbulence. The circular geometry of pipe cross-sections is accommodated with the aid of a bi-polar coordinate system which fits the pipe wall as well as the interface.

Predictions with the technique are compared with the results of other methods and with experimental data for both pipe and rectangular channel geometries. The ability of the method to handle inclined flow is also demonstrated. It is concluded that the treatment of the interface plays an important role in determining the overall behaviour of the flow, and this is reflected in the predicted pressure gradient and hold-up.

1. INTRODUCTION

In the petroleum industry, as well as in other engineering fields, stratified, two-phase flow often occurs. In such an event, determination of the pressure-drop and hold-up in the channel or pipe is essential for design purposes. To this end, several methods, ranging from the purely empirical to the almost wholly analytical have been devised. The former ones suffer obvious limitations, though in the absence of alternative theoretical models in the past, they have been put to wide use. The latter methods offer a more general approach, albeit at the cost of recourse to numerical solution.

The present method builds on two previous works, namely, those of Shoham & Taitel (1984) and Akai *et al.* (1981). In the first of these, the stratified flow of gas and liquid through circular pipes (see figure 1) was considered. The two-dimensional momentum equation for the fully-developed flow of the liquid phase was solved by a finite-difference scheme. The effects of turbulence within the liquid were simulated using the eddy viscosity model, in which a mixing length scale characterizes the turbulent shear stresses. The gas phase, however, was treated as a bulk flow, with the wall and interface shear stresses being calculated from friction factors determined by the average gas velocity. The geometry of the liquid phase was mapped by Shoham & Taitel (1984) in a novel way with the aid of a bi-polar coordinate frame (see figure 2). This system enables the computing mesh to be fitted to the wall of the pipe and to the rectilinear interface simultaneously. The height of the liquid surface is not known in advance, hence the solution has to be iterative, with the mesh being adjusted at each iteration to conform to the position of the interface. Calculations were made for flows in horizontal as well as upward and downward inclined pipes.

In the work of Akai *et al.* (1981), the momentum equations for both the gas and liquid phases were solved, also numerically. Turbulence was accounted for by the use of a modified form of the low Reynolds number version of the k–ϵ model due to Jones & Launder (1973). The work was restricted to planar flow in channels and an application was made to air/mercury flow, for which experimental data were obtained by the same workers.

Both of the above works fall short of addressing the complete problem of stratified flow in inclined pipes and channels. Thus, Shoham & Taitel ignore details of the gas-phase flow from which the pressure gradient is calculated. Reliance on empiricism could not therefore be altogether avoided. More significantly, however, the neglect of the structure of the flow in the gas phase is contrary to the findings of Akai *et al.*, which confirm (both in measurement and in theory) the role

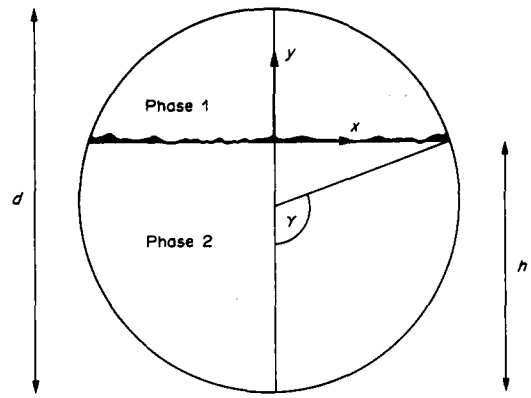

Figure 1. Stratified flow in a circular pipe.

of this phase. Moreover, the mixing length used to determine the eddy viscosity can be defined neither well nor universally in pipe problems, as is indeed explained by Shoham & Taitel (1984).

On the other hand, the work of Akai *et al.* (1981) is confined to planar flow, although, in principle, the governing equations can be generalized to two dimensions. Thus, their calculations were one-dimensional, although the data with which comparison was made actually related to a two-dimensional situation (the channel aspect ratio was only $2\frac{2}{3}$).

In the present paper, a method is outlined for the calculation of stratified flow in inclined pipes and channels of different cross-sectional shapes, and in which both the gas and liquid phases are accounted for fully. The method employs a general curvilinear orthogonal coordinate frame, which

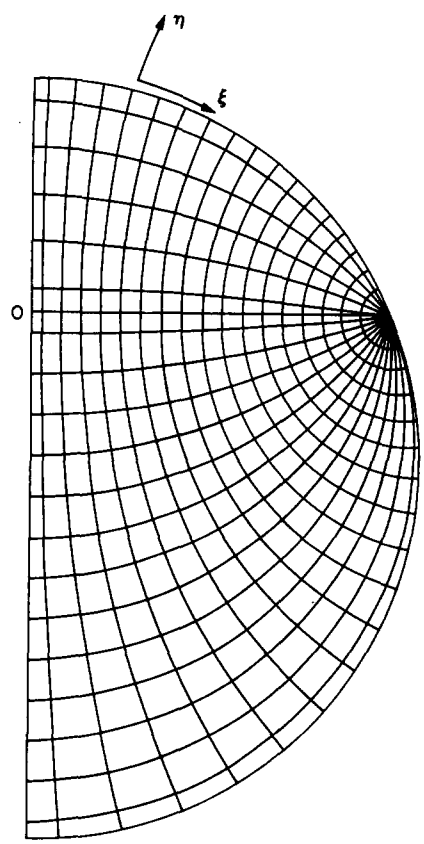

Figure 2. The curvilinear orthogonal mesh defined by bi-polar coordinates.

can handle both circular pipe and rectangular channel geometries, the first being handled with the aid of the bi-polar coordinates proposed by Shoham & Taitel. A new solution algorithm was devised to solve the governing set of equations in this general geometry. Turbulence is accounted for by the use of either the modified form of the low Reynolds number k–ϵ model proposed by Akai *et al.* (1981) or the standard k–ϵ model outlined by Launder & Spalding (1972) for high Reynolds number flow.

The method is applied to several flows in both channels and pipes. The channel flow configuration of Akai *et al.* is computed as a two-dimensional problem and the results are compared with the data and the one-dimensional calculations of these authors. Flow in pipes is treated next, where calculations are compared with: available data; the results of Shoham & Taitel (1984); and calculations performed with the simple method of Taitel & Dukler (1976) for horizontal pipes. Flows in inclined pipes are also computed, and the results are compared with other calculations for plausibility. It should be pointed out that the present work does not delve into the field of turbulence modelling; it merely applies two versions of one particular model (namely, the k–ϵ one). The applicability of this model, which embodies the effective viscosity assumption, is open to question. This has indeed been raised by Fabre *et al.* (1983), who demonstrated that, at least in their experiment, secondary flow can arise in both phases. Also reported in their work is the observation that the incidence of zero shear stress does not necessarily correspond to the occurrence of zero velocity gradient. Both of these phenomena would require more sophisticated turbulence models which solve for the Reynolds stresses directly. Although this is not attempted here, the method presented can be extended with a minimum of effort to incorporate such models.

2. MATHEMATICAL MODEL

2.1. The governing equations

The equations solved are formulated in a general curvilinear orthogonal coordinate system which caters for any orthogonal set, including the bi-polar and cartesian frames used herein for the pipe and channel geometries, respectively. The two independent coordinates are designated ξ and η (as shown, for example, in figure 2), and the equations are presented below in a single form, whether for the gas or the liquid.

The fully-developed momentum equation is

$$\frac{1}{l_\xi l_\eta}\frac{\partial}{\partial \xi}\left(\mu \frac{l_\eta}{l_\xi}\frac{\partial u}{\partial \xi}\right)+\frac{1}{l_\xi l_\eta}\frac{\partial}{\partial \eta}\left(\mu \frac{l_\xi}{l_\eta}\frac{\partial u}{\partial \eta}\right)-\frac{\mathrm{d}p}{\mathrm{d}z}-\rho g \sin\alpha = 0, \qquad [1]$$

where u is the velocity, ρ is the density, $\mathrm{d}p/\mathrm{d}z$ is the pressure gradient in the streamwise direction z, l_ξ and l_η are the metric coefficients which define arc lengths along the ξ- and η-coordinate lines and α is the angle of inclination of the pipe or channel. The quantity μ in [1] is the effective viscosity which is defined as the sum of the molecular viscosity μ_m and a turbulent contribution μ_t, to be obtained from the turbulence model described below.

In this work, two forms of the k–ϵ turbulence model are implemented: the first is the standard version originally formulated for high Reynolds number flow; and the second includes the modifications proposed by Akai *et al.* (1981) for low Reynolds numbers. The equations governing the turbulence kinetic energy, k, and its rate of dissipation, ϵ, both of which characterize turbulence effects, are, respectively

$$\frac{1}{l_\xi l_\eta}\frac{\partial}{\partial \xi}\left(\mu_k \frac{l_\eta}{l_\xi}\frac{\partial k}{\partial \xi}\right)+\frac{1}{l_\xi l_\eta}\frac{\partial}{\partial \eta}\left(\mu_k \frac{l_\xi}{l_\eta}\frac{\partial k}{\partial \eta}\right)+G-\rho\epsilon = 0 \qquad [2]$$

and

$$\frac{1}{l_\xi l_\eta}\frac{\partial}{\partial \xi}\left(\Gamma_\epsilon \frac{l_\eta}{l_\xi}\frac{\partial \epsilon}{\partial \xi}\right)+\frac{1}{l_\xi l_\eta}\frac{\partial}{\partial \eta}\left(\Gamma_\epsilon \frac{l_\xi}{l_\eta}\frac{\partial \epsilon}{\partial \eta}\right)+f_1 C_1 G\frac{\epsilon}{k}-f_2 C_2 \rho\frac{\epsilon^2}{k}+B = 0, \qquad [3]$$

where term B is dependent on the version of the turbulence model used. For the low Reynolds number model proposed by Akai *et al.* (1981) it is

$$B = 2f_2 C_2 \mu_\mathrm{m}\frac{\epsilon}{k}\left[\left(\frac{1}{l_\xi}\frac{\partial\sqrt{k}}{\partial \xi}\right)^2+\left(\frac{1}{l_\eta}\frac{\partial\sqrt{k}}{\partial \eta}\right)^2\right]+2\frac{\mu_\mathrm{m}\mu_\mathrm{t}}{\rho}(\nabla^2 u)^2; \qquad [4]$$

otherwise, $B = 0$. Note that the expression for B is the two-dimensional generalization of the original one which was formulated for boundary layer flow. The coefficients C_1, C_2, f_1 and f_2 are all given in table 1. The effective diffusion coefficient for ϵ, which is Γ_ϵ, is given by

$$\Gamma_\epsilon = \frac{\mu_t}{\sigma} + \mu_m, \quad [5]$$

where σ is a Prandtl number—also specified in table 1.

The turbulent viscosity, μ_t, is related to k and ϵ by

$$\mu_t = f_\mu C_\mu \frac{\rho k^2}{\epsilon}, \quad [6]$$

where f_μ and C_μ are coefficients defined in table 1.

The turbulence Reynolds number, Re_t, in table 1 is defined as

$$\mathrm{Re}_t = \frac{\rho k^2}{\epsilon \mu_m}. \quad [7]$$

Term G in [3] and [4] is the generation of turbulence and is given by

$$G = \mu_t \left[\left(\frac{1}{l_\xi} \frac{\partial u}{\partial \xi} \right)^2 + \left(\frac{1}{l_\eta} \frac{\partial u}{\partial \eta} \right)^2 \right]. \quad [8]$$

Equations [1]–[3] are to be solved for u, k and ϵ for both phases. However, $\mathrm{d}p/\mathrm{d}z$ is also unknown, and so is the height of the interface between the phases, h. To close the set of equations, two additional equations are required; they are

$$\int_{A_L} u \, \mathrm{d}A = Q_L \quad [9]$$

and

$$\int_{A_G} u \, \mathrm{d}A = Q_G, \quad [10]$$

where A is the phase cross-sectional area, Q is the phase flow rate, and subscripts L and G stand, respectively, for liquid and gas.

2.2. *Boundary conditions*

The fact that the flow is symmetric about the vertical mid-plane (or diameter) can be exploited to reduce the computing effort. Thus, only half the channel or pipe needs to be considered. At this plane of symmetry, the appropriate conditions are that the derivatives of all main dependent variables normal to that boundary vanish.

At the pipe wall, different conditions may be imposed, depending on the turbulence model version. For the low Reynolds number version, the conditions proposed by Akai *et al.* (1981) are imposed. Thus

$$u_w = 0, \quad [11]$$

$$k_w = 0 \quad [12]$$

Table 1. Values for the turbulence model coefficients

Coefficient	Value	
	High Re model	Low Re model
C_1	1.44	1.45
C_2	1.92	2.0
f_1	1.0	1.0
f_2	1.0	$1 - 0.3\exp(-\mathrm{Re}_t^2)$
f_μ	1.0	$\exp\left[-2.5\Big/\left(1+\frac{\mathrm{Re}_t}{50}\right)\right]$
C_μ	0.09	0.09
σ	1.3	1.3

and

$$\epsilon_w = \frac{2\mu_m}{\rho}\left(\frac{1}{l_\eta}\frac{\partial\sqrt{k}}{\partial\eta}\right)^2, \qquad [13]$$

where subscript w denotes a wall value. Also, the shear stress at the wall is calculated from

$$\tau_w = \frac{\mu_m}{l_\eta}\frac{\partial u}{\partial\eta}. \qquad [14]$$

When the high Reynolds number model is implemented, the boundary conditions are imposed with the aid of "wall functions" [see, for example, Launder & Spalding (1972)]. Thus, the shear stress is calculated from the log-law:

$$u^+ = \frac{1}{\kappa}\ln \mathrm{E}\Delta\eta^+. \qquad [15]$$

In [15] $\Delta\eta^+$ is the normalized distance $\Delta\eta$ from the wall along the η-coordinate, and u^+ is the velocity normalized by the friction velocity. The constants κ and E take the values of 0.4 and 9.793, respectively. Equation [15] is assumed to be valid in the region between the wall and the first interior grid node, provided that the flow is fully turbulent (judged by the value of $\Delta\eta^+$); otherwise, [14] is used instead. For the turbulence energy and dissipation, the values of k and ϵ at the interior points adjacent to the wall are fixed by

$$k = \frac{\tau_w/\rho}{\sqrt{C_\mu}} \qquad [16]$$

and

$$\epsilon = \frac{(\sqrt{C_\mu}k)^{3/2}}{\kappa\Delta\eta} \qquad [17]$$

2.3. Interface treatment

At the interface, constraints on the behaviour of the dependent variables are needed in both phases. Such behaviour is at present incompletely understood, especially as the interface can often be wavy which makes the prescription of interface conditions an even more tentative affair. It is customary to treat the interface as a moving wall, whereby boundary conditions appropriate to such a wall are imposed. In the case of a wavy interface, it has been sometimes suggested that the interface behaves as a rough wall.

In their work, Akai *et al.* (1981) pointed out the importance of the conditions to be imposed at the interface, especially when this becomes wavy as occurs at high gas flow rates. The present work confirms this conclusion. Unfortunately, Akai *et al.* (1981) could only propose an empirical relationship between the interface waves (characterized by roughness parameters) and the gas Reynolds number. Such a relationship, of course, fits their particular set of data, and cannot therefore be generalized to other flows. Much research is needed, both experimental and theoretical, to arrive at a general model to reflect the effects of these waves, a model which is independent of the geometry of the flow.

In this respect, two main issues in the work of Akai *et al.* (1981) are open to question. These are: (i) the constraint imposed on dissipation; and (ii) the assumption of continuity of k at the interface. The first of these issues is addressed later. As for the second, it can be argued that it is the normal stresses that should be continuous there. If this is true, then the turbulence kinetic energy in the two phases will differ by the ratio of the fluid densities. In this work, however, in order to reproduce the calculations of Akai *et al.* the same condition which assumes the continuity of k has been invoked for the low Reynolds number cases.

As for the treatment of ϵ, and the constraints on k for high Reynolds numbers, several options have been implemented herein, all of which, it must be stressed, are tentative in the absence of a more precise analysis of the flow in the vicinity of the interface.

In conjunction with the low Reynolds number turbulence models, the shear stress at the interface, τ_i, is here calculated from

$$\tau_i = \frac{\mu_m}{l_\eta}\frac{\partial u}{\partial \eta} \qquad [18]$$

for both phases, when the surface is assumed to be smooth. Alternatively, for a wavy interface, the practice of Akai *et al.* (1981) based on a "rough" wall function, is used. Thus, τ_i is evaluated in the gas phase from

$$u^+ = \frac{1}{\kappa}\ln \mathrm{E}_r \frac{\Delta\eta}{\Delta\eta_r}, \qquad [19]$$

where $\Delta\eta_r$ is a characteristic roughness height to be related (empirically) to the waves' structure, and E_r is an empirical constant. For the liquid phase, the shear stress is calculated from

$$\tau_i = \frac{\mu}{l_\eta}\frac{\partial u}{\partial \eta}. \qquad [20]$$

For the present calculations with the wavy interface assumption, the expression for $\Delta\eta_r$ suggested by Akai *et al.* is used.

As for k and ϵ, these are taken as

$$k_i = 0 \qquad [21]$$

and

$$\epsilon_i = \frac{2\mu_m}{\rho}\left(\frac{1}{l_\eta}\frac{\partial\sqrt{k}}{\partial\eta}\right)^2 \qquad [22]$$

for the smooth interface case; and

$$k_i > 0 \qquad [23]$$

and

$$\frac{\partial\epsilon}{\partial\eta} = 0 \qquad [24]$$

for a wavy interface. The finite value for k_i in [23] is again taken from the empirical relation given by Akai *et al.* (1981). However, the boundary condition on ϵ in [24] differs from that perceived to be used by Akai *et al.* (namely [22]). This alternative has been introduced because the former can lead to very small dissipation at the interface (since the gradient of $\sqrt{k}$ may vanish), which results in unrealistically high levels of turbulent viscosity. The zero-gradient condition in [24] stems from the assumption that no diffusion of ϵ occurs across the interface. Other conditions on ϵ, such as those suggested by Celik & Rodi (1984), could also have been imposed; however, such an effort should be included in a separate systemic study which is outside the scope of this work.

When the high Reynolds number model is invoked, the wall function given by [15] is utilized to determine τ_i for both phases, when the interface is smooth; otherwise [19] and [20] are used. The conditions on k and ϵ are derived from wall functions corresponding to [16] and [17] which apply to points adjacent to the interface, whether this is rough or smooth.

3. NUMERICAL METHOD OF SOLUTION

3.1. The computing mesh

The governing equations [1]–[3] are solved numerically by a finite-volume technique. This entails the discretization of the solution domain into a finite number of four-sided cells whose faces coincide with the orthogonal coordinate lines. Values of all computed variables are stored at cell centres (called nodes). A typical cell is shown in figure 3. The interface between the phases is arranged here to be aligned with the boundary between two rows of cells. Since the location of the interface is not known *a priori*, the mesh distribution over the cross-section can only be an outcome of the solution itself. What may be fixed in advance, however, is the number of mesh cells

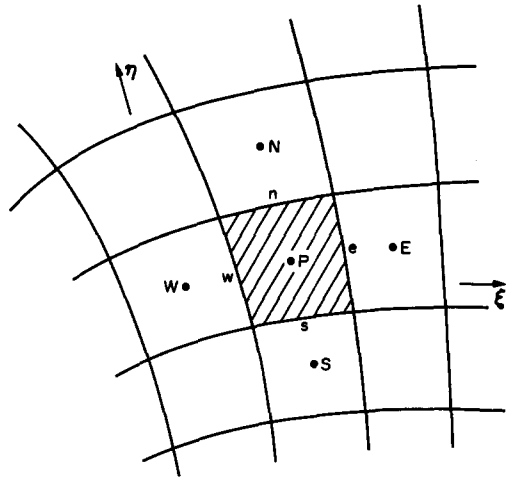

Figure 3. Typical cell in the computing mesh.

covering each phase. The mesh is defined by the specification of the arc lengths of the faces of each cell; these are denoted by $\Delta\xi$ and $\Delta\eta$, respectively, which stand for $l_\xi\, d\xi$ and $l_\eta\, d\eta$. The values of $\Delta\xi$ and $\Delta\eta$ are determined by the coordinate frame used and by how the mesh is distributed.

For the case of channel flow, cartesian coordinates are obviously the most appropriate ones to use, in which case, the cells are of rectangular shape. In this case, $\Delta\xi$ and $\Delta\eta$ can be calculated simply from the breadth and height of the channel, and the number of cells in each direction.

For circular pipe flow, the bi-polar coordinate system, which can accommodate the straight-line configuration of the interface, is utilized, following the practice of Shoham & Taitel (1984). Unlike their work, however, the practice adopted here is based on the use of physical arc lengths instead of the increments $d\xi$ and $d\eta$. These arc lengths are calculated according to the relations given in the appendix. A typical mesh configuration is illustrated in figure 2.

3.2. The finite-difference equations

The finite-difference form of [1]–[3] is obtained by integration of these equations over discrete cells, such as that surrounding node P shown in figure 3. For the purpose of illustration, this process will now be carried out using [1] as an example. The treatment of [2] and [3] follows the same lines.

Multiplication of [1] by $\Delta\xi\ \Delta\eta$ and integration give

$$\left[\left(\mu\frac{\Delta\eta}{\Delta\xi}\right)_e(u_E-u_P)-\left(\mu\frac{\Delta\eta}{\Delta\xi}\right)_w(u_P-u_W)\right]+\left[\left(\mu\frac{\Delta\xi}{\Delta\eta}\right)_n(u_N-u_P)\right.$$
$$\left.-\left(\mu\frac{\Delta\xi}{\Delta_\eta}\right)_s(u_P-u_S)\right]-(\Delta\xi\,\Delta\eta)_P\left(\frac{dp}{dz}\right)-(\Delta\xi\,\Delta\eta)_P\rho g\sin\alpha=0, \quad [25]$$

where the subscripts e, w, n, s, E, W, N and S refer† to either grid nodes or to cell faces, as illustrated in figure 3.

The quantities μ in [25] are taken to be average values which prevail over the whole of the cell face denoted by the subscript and are interpolated from their nodal values. Equation [25] may be re-written as

$$A_P u_P = A_E u_E + A_W u_w + A_N u_N + A_S u_S + S_P, \quad [26]$$

where

$$A_N = \left(\mu\frac{\Delta\xi}{\Delta\eta}\right)_n \quad [27]$$

†These subscripts may be construed as referring to directions East, West, North and South.

with similar expressions applying for the A_S, A_E and A_W coefficients, and where S_P is a source term containing the pressure gradient and gravitational force.

The coefficient A_P is given by

$$A_P = A_E + A_W + A_N + A_S. \quad [28]$$

Equation [26] is symmetric and can be solved by any of the standard schemes for the solution of linear sets of equations.

Similar equations to [26] can be derived for k and ϵ. The only difference in treatment accorded to these equations is that the negative parts of the source terms are preferably shifted to the l.h.s. of the equation where they are treated implicitly; this enhances diagonal dominance and stability, as well as precluding the possibility of negative values for k or ϵ (which is non-physical) being obtained.

Under-relaxation was found to be necessary to promote the stability of the overall solution process. This is introduced in each equation as a pseudo time-dependent term in which the time step size is proportional to A_P. Thus, if the relaxation factor is λ, then A_P is replaced by $(1/\lambda)A_P$ and S_P should be augmented by $[(1-\lambda)/\lambda]A_P$.

3.3. The method of solution

The set of algebraic equations such as [26] are solved iteratively. In each cycle of calculations, the pressure gradient, dp/dz, and the height of the interface, h, are first estimated; the velocity u is then obtained from the momentum equation [26]. The pressure gradient is then adjusted so as to satisfy overall continuity; h is then updated so as to give the correct split between the flow rates of the two phases (an outline of how this is implemented is given below). The k and ϵ fields are computed next from their own equations (like [26]). The cycle is repeated until convergence is attained; this is judged by monitoring the sums of the absolute residuals in the field for each of the variables.

The calculation of the pressure gradient in each iteration is performed according to the following procedure. At the beginning of the cycle, the pressure gradient is estimated (from the previous iteration). The momentum equation [26] is solved to give the velocity field over the whole cross-section. This velocity field will not give the correct total flow rate, unless the solution is converged, since the value of dp/dz is only an estimate. The pressure gradient in the momentum equation [25] is now updated such that the new velocity field denoted by u satisfies the overall flow rate; thus

$$\sum_{G+L} a_p u_p = Q_G + Q_L \quad [29]$$

where the summation is over all cells in the domain, a_p is the cell area, and Q_G and Q_L are the flow rates of the gas and liquid phases, respectively.

Next, the calculation of h, the height of the interface, is dealt with. This is based on the fact that h provides a measure of the split between the flow rates of the individual phases. Hence, h must satisfy the flow rate of one of the phases; here, the flow rate of the gas is considered.

Unless the solution is converged, the gas velocity and flow area (which depends on h) will not satisfy the flow rate of gas. The value of h is now adjusted, such that the new cell areas, denoted by a, satisfy the relationship

$$\sum_{G} a_p u_p = Q_G, \quad [30]$$

where the summation is over all cells in the gas phase.

4. RESULTS

4.1. Channel flow

The flow geometry in question is that presented by Akai *et al.* (1981), in which the phases are air and mercury, flowing at low Reynolds numbers in a rectangular channel with an aspect ratio

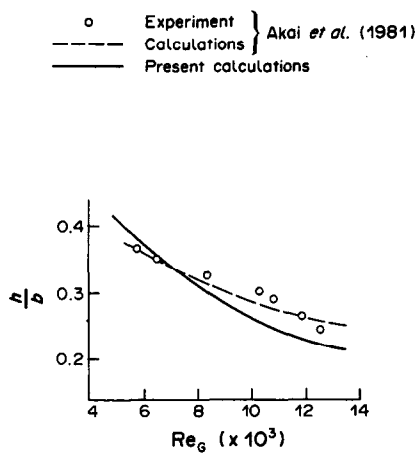

Figure 4. Film thickness in channel flow.

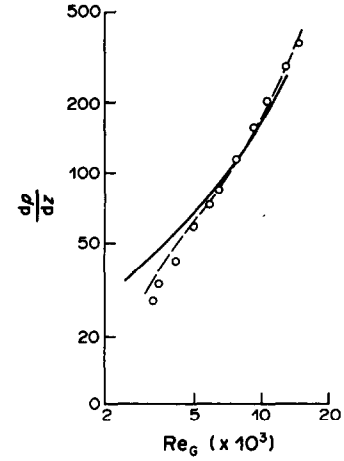

Figure 5. Pressure gradient in channel flow.

of $2\frac{2}{3}$:1. Despite this small ratio, the calculations carried out by these workers were for planar geometry. The results were compared with data obtained from their own experiment.

Here, the same flow is computed over the two-dimensional cross-section in order to account for lateral variations as well as for the shear stresses on the side wall. The present computations are different in other aspects also. The zero-gradient condition on ϵ at the wavy interface [24] is used here in place of condition [22], which is the one perceived to be used by Akai *et al.* The latter condition applies at a smooth wall, well into the sublayer, whereas the actual case is that of highly agitated flow with a finite k at the interface.

The other major difference between the two calculations is the use of the high Reynolds number model in the present work, when the Reynolds number exceeds 10^4, as happens with the gas phase in certain cases. All computed cases were with a liquid Reynolds number of 8.04×10^3.

Figure 4 displays the computed film thickness as a function of the gas Reynolds number, while figure 5 shows the same for the pressure gradient. The results are compared against the calculations and data of Akai *et al.* (1981). The latter calculations are with the wavy interface treatment throughout, while the present results are obtained from assuming a smooth interface up to a gas Reynolds number of 5000, and a rough one thereafter. The empirical formulae given in the cited reference for the roughness height and the interface turbulence energy are also employed here.

The comparison shows that a reasonable match with the data is obtained, except at the lower Reynolds numbers when the computed pressure gradients overestimate the data considerably. It is thought that at these low Reynolds numbers (2000–4000), the k–ϵ model fails to capture the correct turbulence levels, which is not surprising since transition takes place in this regime. It is not clear, however, what modifications Akai *et al.* introduced into their calculations for gas

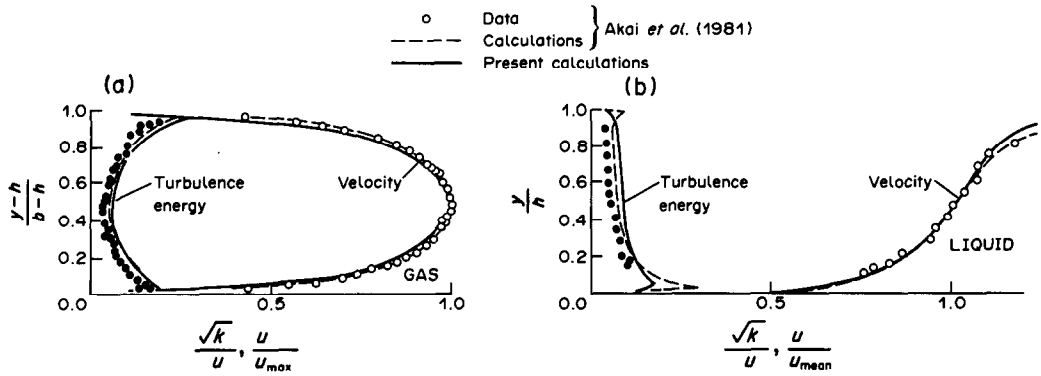

Figure 6. Velocity and turbulence energy profiles in channel flow at $Re_G = 2.34 \times 10^3$.

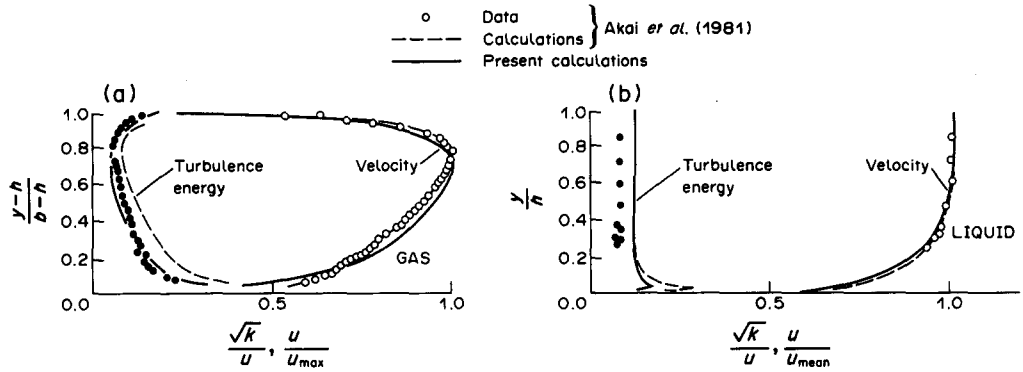

Figure 7. Velocity and turbulence energy profiles in channel flow at $Re_G = 1.32 \times 10^4$.

Reynolds numbers <5000, as their computations are apparently based on the wavy interface treatment, when clearly this is not realistic.

Figures 6 and 7 compare the profiles of the velocity and kinetic energy (normalized in the same fashion as by Akai *et al.*) for each phase; the first figure is for a gas Reynolds number of 2.34×10^3, and the second is for 1.32×10^4. The level of agreement with the data is satisfactory. It was found that the effects of the end walls are indeed negligible, thus vindicating Akai *et al.* (1981) in their one-dimensional approach.

The present computations were performed with 80 nodes in the vertical direction (with 30 being in the liquid phase) and 10 in the lateral direction.

4.2. Pipe flow

The method is here applied to the calculation of gas/liquid flow in circular, horizontal and inclined pipes. Comparison of the results will be made against data, the calculations of Shoham & Taitel (1984), whose method solves for details of the liquid phase only, and the simpler model of Taitel & Dukler (1976). All the calculations made with the present method used the smooth interface treatment, in the absence of knowledge of the wave characteristics at the interface.

First considered is the horizontal pipe case. Several experiments had been conducted in the past for horizontal flow, using different configurations. The data are usually presented in the form of plots of E_L, the fraction of cross-sectional area occupied by the liquid phase, and of ϕ_G, which is defined as

$$\phi_G = \sqrt{\frac{(dp/dz)_{tp}}{(dp/dz)_{Gs}}},$$

where the subscript tp denotes the two-phase case and Gs stands for the single-phase flow of gas. These quantities are plotted against the Lockhart–Martinelli parameter, χ, which is defined as

$$\chi = \sqrt{\frac{(dp/dz)_{Ls}}{(dp/dz)_{Gs}}},$$

where the subscript Ls denotes single-phase liquid flow.

Figures 8 and 9 display such plots. The shaded area covers the scattered data obtained from the various experiments. These are due to Cheremisinoff & Davis (1979). Agrawal *et al.* (1973), Govier & Omer (1962), Hoogendoorn (1959) and Bergelin & Gazley (1949). Also shown in these figures are: the present predictions; those of Shoham & Taitel (1984); and the predictions, by the latter authors, using the Taitel & Dukler (1976) model. The results of Shoham & Taitel (1984) are based on a wavy interface empirical correlation for the interface shear stress. The present calculations were made with air and water in a 2.54 cm dia pipe. The figures show good correlation between data and predictions. It is somewhat surprising, however, to find that the present calculations agree more with the results of the Taitel & Duckler (1976) model than with those of Shoham & Taitel (1984) at high values of χ. At lower values, however, when surface waves become prominent, the

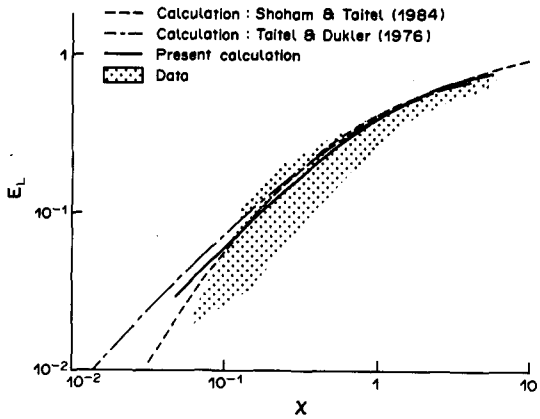

Figure 8. Liquid hold-up in a horizontal pipe.

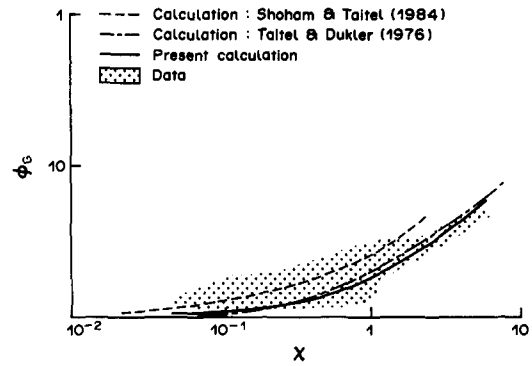

Figure 9. Pressure gradient in a horizontal pipe.

departure between these calculations is to be expected due to the differences in the treatments of the interface. Nevertheless, the agreement is good considering the fundamental differences between all these methods.

The velocity contours for both gas and liquid in the cross-section of a pipe of 2.54 cm dia are presented next. The fluids are air and water flowing at superficial velocities of 1.0 and 0.1 m/s, respectively. Three pipe inclinations are considered: horizontal, upward inclined ($+10°$) and downward inclined ($-10°$); these cases were also computed by Shoham & Taitel (1984). Figures 10–12 display these contours for the respective cases.

A comparison between the presently predicted contours and those of Shoham & Taitel (not shown) reveal certain similarities and some differences. The main departure between the two calculations is that, unlike the cited work, the present method does not predict reverse flow for the upward inclined pipe. This illustrates how important solving for the gas can be. It is obvious that, for this case, the gas turbulence, which affects the interface shear stress, plays a major role in preventing liquid flow reversal. Indeed, the computed interface shear stresses were about five times those obtained from the empirical formula employed by Shoham & Taitel (1984). In order to verify this hypothesis, a computation was made in which the flow of both phases was assumed to be laminar; as anticipated, reverse flow occurred.

The values of h/d and ϕ_G computed for these cases are compared with the results of Shoham & Taitel (1984) and of the model of Taitel & Dukler (1976) in table 2. Agreement is close, with the exception of the downward inclined case. Here, again, the reason behind this difference is the

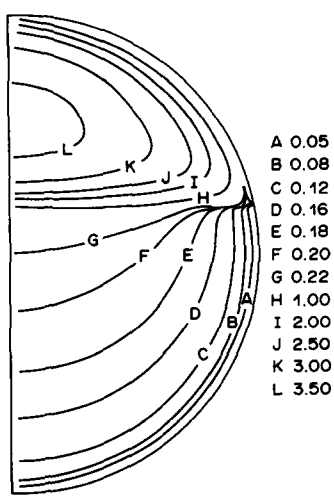

Figure 10. Velocity distribution in a horizontal pipe—contours in m/s.

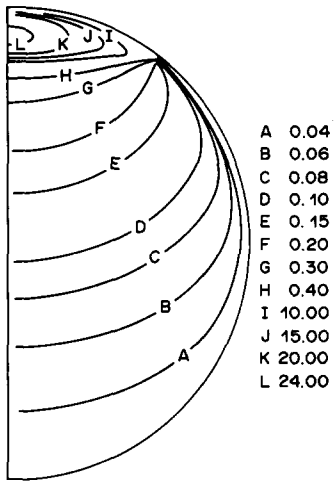

Figure 11. Velocity distribution in an upward inclined pipe—contours in m/s.

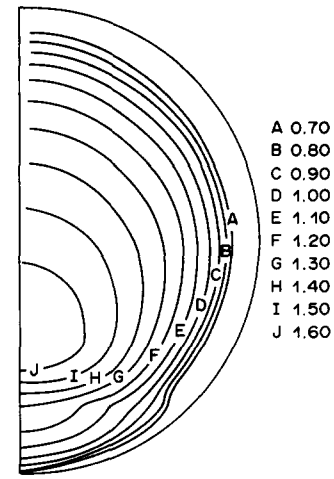

Figure 12. Velocity distribution in a downward inclined pipe—contours in m/s.

inclusion of the gas phase in the present analysis, which is expected to yield more accurate results for the shear stresses acting on this phase. The other methods calculate these stresses based on the assumption that the gas velocities are much greater than the liquid ones. In the downward inclined flow, because of the differential effect of gravity, the phase velocities are almost equal, thus grossly violating the above assumption. It is therefore expected that the present calculations should prove to be the more realistic of the three.

The predictions were performed with a 40 × 40 mesh. In order to verify the independence of the solution on the mesh size, calculations were also made with a grid of 20 × 20. These gave negligible differences from the finer mesh results, hence proving grid independence. Typically, a 20 × 20 mesh calculation requires 26 CPU seconds on the CYBER 855 machine to converge to a tolerance of 10^{-3} on normalized residuals.

5. CONCLUSIONS

A method for the calculation of fully-developed, stratified, two-phase flow in inclined channels and pipes has been presented. The method includes two versions of the k–ϵ turbulence model, for high and low Reynolds numbers, respectively. It is based on the solution of the basic governing differential equations numerically, using a finite-volume technique, and a curvilinear orthogonal mesh which caters for both rectangular and circular cross-sections; a bi-polar coordinate system is utilized for the latter. The algorithm solves the set of finite-difference equations in an iterative loop, in which the equations are solved sequentially. The pressure gradient is computed from the requirement that the velocity field in both phases must satisfy the total flow rate, while the interface height is calculated such that the correct split between the flow rates of the two phases is obtained.

The method was applied to both channel and pipe flow cases, and the results compared with available data and other calculations. Agreement is found to be close. The merit of the method

Table 2. Computed surface height and pressure gradient in an inclined pipe

Inclination angle	Quantity	Present calculation	Taitel & Dukler (1976)	Shoham & Taitel (1984)
0°	h/d	0.59	0.59	0.66
	ϕ_G	3.7	3.7	5.5
+10°	h/d	0.89	0.89	0.89
	ϕ_G	37.0	38.0	38.0
−10°	h/d	0.16	0.17	0.18
	ϕ_G	0.73	1.86	1.85

in including the gas phase in the analysis is highlighted in some of the applications where empirical correlations normally used for the gas phase become invalid.

The question of what boundary conditions to impose on k and ϵ at the interface, especially in the presence of waves, remains unresolved. These need further examination and assessment. In particular, the boundary constraint on ϵ suggested by Akai *et al.* (1981) was found to be somewhat unreliable; it is this which prompted the introduction in this work of the zero-gradient boundary constraint in its place. A further study of these conditions is warranted.

Acknowledgements—The author wishes to thank Shell for their support, Dr R. V. Oliemans of Shell-KSLA for his interest in the work and Dr B. A. Younis for his valuable assistance in obtaining the results.

REFERENCES

AGRAWAL, S. S., GREGORY, G. A. & GOVIER, G. W. 1973 An analysis of horizontal stratified two-phase flow in pipes. *Can. J. chem. Engng* **51,** 280–286.

AKAI, M., INOUE, A. & AOKI, S. 1981 The prediction of stratified two-phase flow with a two-equation model of turbulence. *Int. J. Multiphase Flow* **7,** 21–39.

BERGELIN, O. P. & GAZLEY, C. 1949 Concurrent gas–liquid flow in horizontal tubes. *Proc. Heat Transfer Fluid Mech. Inst.* **29,** 5–40.

CELIK, I. & RODI, W. 1984 Simulation of free surface effects in turbulent channel flows. *Physico-Chem. Hydrodynam. J.* **5,** 217–227.

CHEREMISINOFF, N. P. & DAVIS, E. J. 1979 Stratified turbulent–turbulent gas–liquid flow. *AIChE Jl* **25,** 48–56.

FABRE, J., MASBERNAT, L. & SUZANNE, C. 1983 New results on the structure of stratified gas–liquid flow. In *Advances in Two-phase Flow and Heat Transfer*, Vol. 1 (Edited by KAKAÇ, S. & ISHII, M.), pp. 135–154. Martinus Nijhoff, The Hague.

GOVIER, G. W. & OMER, M. M. 1962 The horizontal pipeline flow of air–water mixtures. *Can. J. chem. Engng* **40,** 93–104.

HOOGENDOORN, C. L. 1959 Gas–liquid flow in horizontal pipes. *Chem. Engng Sci.* **9,** 205–217.

JONES, W. P. & LAUNDER, B. L. 1973 The calculation of low-Reynolds number phenomena with a two-equation model of turbulence. *Int. J. Heat Mass Transfer* **16,** 1119–1130.

LAUNDER, B. L. & SPALDING, D. B. 1972 *Mathematical Models of Turbulence*. Academic Press, New York.

SHOHAM, O. & TAITEL, Y. 1984 Stratified turbulent–turbulent gas–liquid flow in horizontal and inclined pipes. *AIChE Jl* **3,** 377–385.

TAITEL, Y. & DUKLER, A. E. 1976 A model for predicting flow regime transitions in horizontal and near horizontal gas–liquid flow. *AIChE Jl* **22,** 47–55.

APPENDIX

The Bi-polar Coordinate System

Given the pipe geometry of figure 1, a bi-polar coordinate frame can be defined by

$$x + iy = ic \operatorname{cotan}\left(\frac{\eta + i\xi}{2}\right), \qquad [A.1]$$

where i is $\sqrt{-1}$, ξ and η are the coordinate directions shown in figure 2, and c is a constant. It can be shown from [A.1] that

$$x = \frac{-c \sinh \xi}{\cosh \xi - \cos \eta} \qquad [A.2]$$

and

$$y = \frac{c \sin \eta}{\cosh \xi - \cos \eta}. \qquad [A.3]$$

The metric coefficients can be derived from

$$l_\xi = \sqrt{\left(\frac{\partial x}{\partial \xi}\right)^2 + \left(\frac{\partial y}{\partial \xi}\right)^2} \qquad [A.4]$$

with a similar expression for l_η. Such relations lead to

$$l_\xi = l_\eta = \frac{|c|}{\cosh \xi - \cos \eta}. \qquad [A.5]$$

The arc length along ξ-direction lines, $\Delta\xi$, is given by

$$\Delta\xi = \int_{\xi_1}^{\xi_2} l_\xi \, d\xi = \int_{\xi_1}^{\xi_2} \frac{|c|}{\cosh \xi - \cos \eta} \, d\xi.$$

Integration gives:

$$\Delta\xi = \frac{2|c|}{\sin \eta}\left[\tan^{-1}\left(\sqrt{\frac{1+\cos\eta}{1-\cos\eta}}\tanh\frac{\xi}{2}\right)\right]_{\xi_1}^{\xi_2} \qquad [A.6]$$

for $\cos \eta \neq -1$; and

$$\Delta\xi = |c|\left[\tanh\frac{\xi}{2}\right]_{\xi_1}^{\xi_2} \qquad [A.7]$$

for $\cos \eta = -1$; which corresponds to the interface, i.e. $y = 0$.

The arc length along the η-direction lines, $\Delta\eta$, is

$$\Delta\eta = \int_{\eta_1}^{\eta_2} l_\eta \, d\eta = \int_{\eta_1}^{\eta_2} \frac{|c|}{\cosh \xi - \cos \eta} \, d\eta$$

which leads to:

$$\Delta\eta = \frac{2|c|}{\sinh \xi}\left[\tan^{-1}\left(\sqrt{\frac{\cosh\xi+1}{\cosh\xi-1}}\tan\frac{\eta}{2}\right)\right]_{\eta_1}^{\eta_2} \qquad [A.8]$$

for $\cosh \xi \neq 1$; and

$$\Delta\eta = -|c|\left[\operatorname{cotan}\frac{\eta}{2}\right]_{\eta_1}^{\eta_2} \qquad [A.9]$$

for $\cosh \xi = 1$; which corresponds to the vertical diameter i.e. $x = 0$.

Specification of ξ_1, ξ_2 etc. on the interface therefore determines the grid distribution in the ξ-direction, while the definition of η_1, η_2 etc. on the vertical diameter determines the mesh distribution in the η-direction. The arc lengths are then calculated from [A.6] and [A.8].